Cuadernos de Investigación Geográfica *Geographical Research Letters*	2025	Nº 51 (1)	pp. 145-169	EISSN 1697-9540

http://doi.org/10.18172/cig.6415

ADVANCEMENTS IN HIGH-RESOLUTION LAND USE MAPPING: METHODOLOGIES AND INSIGHTS FROM THE RETHINKACTION H2020 PROJECT

CHRISTOPH CORREIA, JESÚS ORTUÑO CASTILLO*, MARTA TORO BERMEJO, PATRICIA PÉREZ RAMÍREZ*

Remote Sensing and Geospatial Analytics Division, GMV, Madrid, Spain.

ABSTRACT. Land use and land cover (LULC) mapping is essential for land-based climate change adaptation and mitigation strategies. This study presents the development of 10-meter high-resolution (HR) land use maps within the RethinkAction H2020 project, aimed at enhancing spatial planning for climate mitigation and adaptation. The methodology integrates multi-source remote sensing data, machine learning classification techniques, and auxiliary datasets to generate accurate and transferable land use classifications across six European bioclimatic regions. The study employs Sentinel-2 and Landsat-8 imagery, using supervised classification with Random Forest (RF) and Geographic Object-Based Image Analysis (GEOBIA) to enhance accuracy and minimize spectral confusion. This approach resulted in the creation of twelve HR land use maps at two classification levels, covering six case study (CS) areas. A key contribution of this research is the generation of suitability maps, which assess the potential for implementing land-based mitigation and adaptation solutions (LAMS) such as reforestation, water harvesting, and photovoltaic energy development. This study highlights the importance of integrating remote sensing, machine learning, and spatial analysis to support evidence-based decision-making in land use planning, offering a scalable and replicable methodology for detailed LULC classification.

Avances en la cartografía de alta resolución de usos del suelo: metodologías y aprendizajes del proyecto H2020 RethinkAction

RESUMEN. La cartografía de uso y cobertura del suelo (LULC, por sus siglas en inglés) es fundamental para las estrategias de adaptación y mitigación del cambio climático basadas en el territorio. Este estudio presenta el desarrollo de mapas de uso del suelo de alta resolución (HR) a 10 metros en el marco del proyecto RethinkAction H2020, con el objetivo de mejorar la planificación espacial orientada a la mitigación y adaptación climática. La metodología integra datos de teledetección, técnicas de clasificación mediante aprendizaje automático y conjuntos de datos auxiliares para generar clasificaciones precisas y transferibles del uso del suelo en seis regiones bioclimáticas europeas. El estudio emplea imágenes de Sentinel-2 y Landsat-8, utilizando clasificación supervisada con Random Forest (RF) y análisis geográfico basado en objetos (GEOBIA) para mejorar la precisión y reducir la confusión espectral. Este enfoque dio lugar a la creación de doce mapas HR de uso del suelo en dos niveles de clasificación, abarcando seis áreas de estudio de caso (CS). Una contribución clave de esta investigación es la generación de mapas de idoneidad, que evalúan el potencial para implementar soluciones de mitigación y adaptación basadas en el suelo (LAMS), como la reforestación, la captación de agua y el desarrollo de energía fotovoltaica. Este estudio subraya la importancia de integrar teledetección, aprendizaje automático y análisis espacial para respaldar la toma de decisiones fundamentadas en la planificación del uso del suelo, ofreciendo una metodología escalable y replicable para la clasificación detallada de LULC.

Keywords: Land Use Maps, GEOBIA, Spatial Analysis Remote Sensing Techniques, High-Resolution Mapping.

Palabras clave: Usos del suelo, GEOBIA, Análisis espacial, Teledetección, Cartografía de alta resolución.

Received: 29 October 2024

Accepted: 27 June 2025

***Corresponding author:** Patricia Pérez Ramírez and Jesús Ortuño Castillo, Remote Sensing and Geospatial Analytics Division, GMV, Madrid, Spain. Email address: ppramirez@gmv.com; jortuno@gmv.com

1. Introduction

Land use mapping is an invaluable tool in the realm of climate change mitigation, serving as a foundational element for greenhouse gas inventories (ESA, 2024). It enables the identification of regions rich in carbon stocks, such as forests, peatlands, and wetlands. These areas are critical for devising strategies aimed at curtailing deforestation and degradation, thereby making significant contributions to climate change mitigation efforts. The precise delineation of land use through mapping is essential for pinpointing these carbon-dense areas, facilitating targeted conservation and management practices that help in reducing atmospheric carbon levels.

Furthermore, land use maps are essential tools in the siting of renewable energy projects, such as solar and wind farms, as they help identify suitable locations while considering environmental, social, and economic factors. Scientific studies have emphasized the importance of integrating land use considerations into renewable energy planning to minimize conflicts and promote sustainable development (Patankar, 2022). The selection of appropriate locations for these projects is crucial to ensure that they have minimal ecological impacts while maximizing energy production. Detailed land use information provided by mapping enables stakeholders to identify sites that are not only suitable for renewable energy generation but also are in harmony with the surrounding environment, thus balancing energy needs with ecological conservation.

LULC mapping is essential for environmental monitoring, urban planning, agriculture, and climate change mitigation. Advances in remote sensing and machine learning have significantly improved classification accuracy, enabling large-scale high-resolution mapping (Gong *et al.*, 2020). Studies have demonstrated its effectiveness in deforestation monitoring (Hansen *et al.*, 2013), urban expansion tracking (Zhao *et al.*, 2022), and land-use planning for renewable energy (Patankar *et al.*, 2022). The use of multi-temporal Sentinel-2 and Landsat-8 imagery has further enhanced spatial and temporal change detection (Holtgrave *et al.*, 2020).

LULC maps are widely used in agriculture and resource management to monitor crop phenology, irrigation, and soil degradation. Remote sensing has been applied to detect irrigated croplands (Wu *et al.*, 2011) and analyze crop phenology in China (You *et al.*, 2013), highlighting the value of HR land classification for precision agriculture and sustainable land-use planning. Additionally, spectral indices like NDVI, NDMI, and NDWI effectively distinguish vegetation types and water bodies in complex landscapes (Costa *et al.*, 2022).

Advancements in machine learning have improved LULC classification accuracy. Random Forest (RF), introduced by Breiman (Breiman, 2001), is widely used for its robust performance with large datasets and ability to reduce overfitting. Studies have shown its effectiveness in multi-temporal and multi-spectral land cover classification (Ramezan *et al.*, 2021; Tang *et al*., 2021). The integration of GEOBIA with RF further enhances accuracy by reducing salt-and-pepper noise and improving object-based classification, making it a preferred method for HR land cover studies.

The aim of this paper is to detail the process followed in Rethink Action H2020 Project to develop 10-meter high resolution (HR) land use maps for six case study (CS) areas and highlights the significance of developing land use maps and spatial analyses for the strategic allocation of land uses in

different geographical areas. The objective of the selected methodology was to provide detailed land use maps which are aligned with the needs expressed by other project tasks (mainly regarding land use classes), are replicable in other potential CSs, and ensures the use of common inputs wherever feasible, considering the resources allocated for this activity within the project.

2. The RethinkAction project

The RethinkAction project is a European initiative aimed at addressing climate change through innovative land use strategies. Funded by the Horizon 2020 program, it brings together thirteen partners from nine countries, integrating expertise from diverse fields such as social sciences, environmental sciences, and information technology.

Launched in October 2021, RethinkAction is developing a decision-making platform designed for policymakers, stakeholders, and citizens. This platform provides clear, actionable insights on climate change, emphasizing the crucial role of land use in sustaining life and achieving climate objectives. It also raises awareness about how individual and collective behavioral changes can shape land use patterns, thereby encouraging active participation in climate action.

A key component of the project is the creation of HR land use maps, which serve as the backbone for further analysis and decision-making. These HR land use maps are used in the project to create suitability maps through a multi-criteria spatial analysis. These maps support land use allocation modeling within the local System Dynamics (SD) models, whose goal is to define the adaptation and mitigation potential of each selected Land-based Adaptation and Mitigation Solution (LAMS).

2.1. Case Studies (CS)

The HR land use maps have been created for the 6 CSs defined by RethinkAction (Figure 1). The CSs comprise relevant and representative examples of EU based territories with a variety of climate change impacts and land system pressures. The variety and representativeness of the CSs selected ensure a broad replicability of RethinkAction solutions across Europe. The spatial boundaries of the CSs have been defined following the Nomenclature of territorial units for statistics (NUTS) which is a geographical system, according to which the territory of the European Union is divided into hierarchical levels. The three hierarchical levels are known as NUTS -1, NUTS -2 and NUTS -3. RethinkAction uses NUTS-2 and NUTS-3 to define the CSs:

- Boreal CS (CS1): Gotland Region, Sweden (NUTS-3), 3142 km2.
- Atlantic CS (CS2): Tarn-et-Garonne, France (NUTS-3), 3730 km2.
- Continental CS (CS3): Southern Great Plain, Hungary (NUTS-2), 18332 km2.
- Alpine CS (CS4): Valle d'Aosta Region, Italy (NUTS-2), 3261 km2.
- Mediterranean CS (CS5): Almería province, Spain (NUTS 3), 8776 km2.
- Macaronesia CS (CS6): Azores archipelago, Portugal (NUTS 2), 2302 km2.

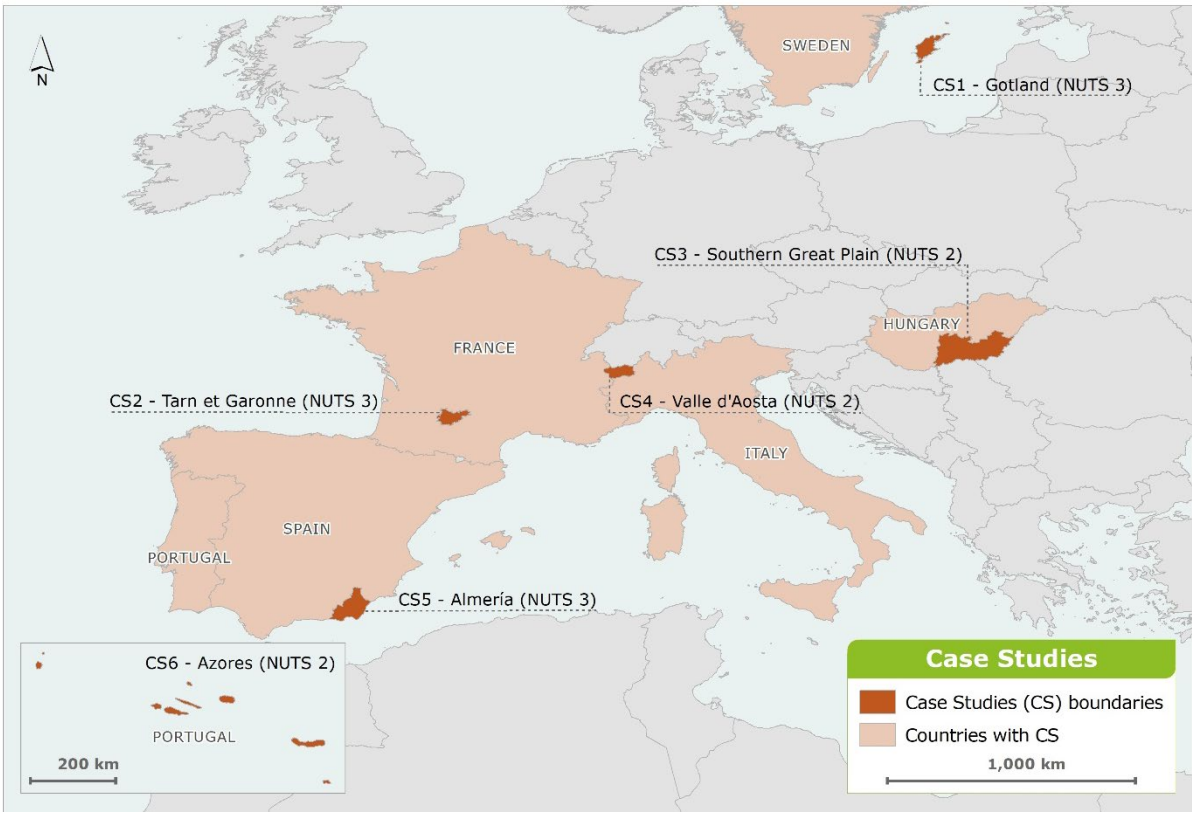

Figure 1.

3. Data and methodology

3.1. Land use classes

The land use maps constitute the baseline for RethinkAction to study and assess relevant actions and solutions that are related to land use. The land use maps are the baseline for other RethinkAction tasks, mainly for the development of the local SD models. The design of the land use maps has taken into consideration the requirements provided by the SD models developers and other related project tasks. One of the main requirements was the request of specific land use classes which has resulted in the development of two different levels of land use maps: Level 1 (L1) and Level 2 (L2).

Land use maps L1 is the basic version of the land use maps which includes 12 land use classes. The definition of the L1 of the HR land use maps was based on the requirements mainly provided by the RethinkAction modellers that need the defined land use classes as inputs of the local SD models. Land use maps L2 is an extended version of the L1 land use maps including additional classes requested by the project that were considered for the development of the suitability maps generated for the project as well and based on the HR land use maps too. L2 provides 21 different classes: the ones included in L1 plus the disaggregation of Urban Land, Water and Other Land classes. The list of the classes of the HR land use maps L1 and L2 is included in Table 1.

Table 1. Land use classes of the HR land use maps L1 and L2.

Land use maps L1	**Land use maps L2**
Rainfed Cropland	Rainfed Cropland
Irrigated Cropland	Irrigated Cropland
Forest Managed	Forest Managed
Forest Primary	Forest Primary

Forest Plantation	Forest Plantation
Shrubland	Shrubland
Grassland	Grassland
Wetland	Wetland
Urban Land	Continuous Urban Land
	Discontinuous Urban Land
	Industrial/Commercial Units
	Roads
	Mining
Solar Land	Solar Land
Water	Water
	Water bodies
	Permanent Snow
Other Land	Bare Rock/Soil
	Sparsely Vegetated
	Beaches/Dunes/Sand

3.2. Input data

The input data for obtaining the required land use classifications consist of a combination of freely available satellite imagery and auxiliary data for automatic training site extraction. Specifically:

1. Sentinel-2 and Landsat-8 satellite imagery serve as the primary classification features.
2. A multi-temporal approach was adopted, using four trimestral Sentinel-2 composites (10 bands each) from 2021 and 2022 to represent an agricultural year.

In five of the six CS areas (excluding the Azores archipelago), the four trimestral 10-band Sentinel-2 composites (with 10 m spatial resolution) were processed in Google Earth Engine (GEE). Image compositing was applied to reduce outliers, shadows, and cloud cover, ensuring more accurate land cover classification (Beshir *et al.*, 2023).

Table 2 presents the technical specifications of the satellite data used.

Table 2. Satellite data specifications.

CS	Sensor	Bands	Central Wavelength (µm)	Spatial resolution (m)	Composite spatial resolution (m)	Time frame
CS1 CS2 CS3 CS4 CS5	Sentinel 2	Band 2 - Blue	0.49	10	10	1st trimester - 01/01/2022 - 31/03/2022 2nd trimester - 01/04/2022 - 30/06/2022 3rd trimester - 01/07/2021 - 31/08/2021 4th trimester - 01/09/2021 - 12/12/2021
		Band 3 - Green	0.56	10		
		Band 4 - Red	0.665	10		
		Band 5 - Vegetation Red Edge	0.705	20		
		Band 6 - Vegetation Red Edge	0.74	20		
		Band 7 - Vegetation Red Edge	0.783	20		
		Band 8 - NIR	0.842	10		
		Band 8A - Narrow NIR	0.865	20		
		Band 11 - SWIR I	1.61	20		
		Band 12 - SEIW II	2.19	20		

CS6o	Sentinel 2	Band 2 - Blue	0.49	10		1st trimester - 01/01/2022 - 31/03/2022 2nd trimester - 01/04/2022 - 30/06/2022 3rd trimester - 01/07/2021 - 31/08/2021 4th trimester - 01/09/2021 - 12/12/2021
		Band 3 - Green	0.56	10		
		Band 4 - Red	0.665	10		
		Band 8 - NIR	0.842	10		
		Band 11 - SWIR I	1.61	20		
		Band 12 - SEIW II	2.19	20		
	Landsat 8	Band 2 - Blue	0.482	30		
		Band 3 - Green	0.561	30		
		Band 4 - Red	0.655	30		
		Band 5 - NIR	0.865	30		
		Band 6 - SWIR I	1.609	30		
		Band 7 - SWIR II	2.2	30		

In the Azores islands persistent cloud cover avoided cloud-free Sentinel-2 image composites. Therefore, Landsat 8 was also used in the Azores archipelago CS to cover this lack of cloud-free images. Sentinel 2 and Landsat 8 surface reflectance data were merged and downscaled to 10 meters. This resulted into four cloud-free median composites, one per trimester (2021 – 2022), each with 6 bands: Blue, Green, Red, Near InfraRed (NIR), Short-Wave InfraRed1 (SWIR1) and Short-Wave InfraRed2 (SWIR2).

To complete the set of classification features, the following spectral indices composites (using maximum values) were computed in GEE for each CS and each trimester: Normalized Difference Vegetation Index (NDVI), Bare Soil Index (BSI), Moisture Stress Index (MSI), Normalized Difference Moisture Index (NDMI), Normalized Difference Snow Index (NDSI), and Normalized Difference Water Index (NDWI).

For the extraction of training sites several datasets from the Copernicus Land Monitoring Service (CLMS) were used. The most recent datasets of the products were used, which are dated from 2018. To complement these datasets and to guarantee efficient training site extraction (see section Training site extraction), local land use/land cover data and different thematic land masks were requested and provided by the CS leaders. Other additional datasets such as the Solar Land feature from OpenStreetMap (OSM) as well as the 2015 Global Forest Management data (GFMD) were also used for training site extraction. Table 3 shows a summary of ancillary data used for this purpose.

Table 3. Ancillary data.

Data provider	Dataset	Date	CS	Source
CLMS	Corine Land Cover (CLC)	2018	All	*https://land.copernicus.eu/pan-european/high-resolution-layers*
	Imperviousness Density (IMD)	2018	All	
	Impervious Built-up (IBU)	2018	All	
	Dominant Leaf Type (DLT)	2018	All	
	Tree Cover Density (TCD)	2018	All	
	Grassland (GRA)	2018	All	
	Water and Wetness (WAW)	2018	All	
	Urban Atlas (UAtlas)	2018	CS3 CS4 CS5 CS6	*https://land.copernicus.eu/local*
	Natura 2000 (NK200)	2018	All	
National Geographic Information Center (CNIG) [Centro Nacional de Información Geográfica]	Sistema de Información sobre Ocupación del Suelo de España (SIOSE)	2018	CS5	*http://centrodedescargas.cnig.es/CentroDescargas/catalogo.do?Serie=SIOSE*
	Superficies de Secano (Rainfed)	2013		

Ministry of Agriculture of Hungary (AM) [Agrárminisztérium]	Ökoszisztéma-alaptérkép/ Ecosystem Map of Hungary (OSZ)	2015-2017	CS3	*http://alapterkep.termeszetem.hu/*
Swedish Environmental Protection Agency [Naturvårdsverket]	Naturvårdsverket/National Land Cover Database (NMD)	2018	CS1	*https://www.naturvardsverket.se/en/services-and-permits/maps-and-map-services/national-land-cover-database/*
National Institute of Geographic and Forest Information (IGN-F) [Institut national de l'information géographique et forestière]	Occupation du sol/Land cover map (LUF)	2013	CS2	*https://www.data.gouv.fr/fr/datasets/occupation-du-sol-2013-tarn-et-garonne/*
National Geographic Information System (SNIG) [Sistema Nacional de Informação Geográfica]	Carta de Ocupação do Solo Açores/Land Cover Map Azores (COS)	2018	CS6	*http://ot.azores.gov.pt/COSA-2018.aspx*
Institute for the Financing of Agriculture and Fisheries (IFAP) [Instituto de Financiamento da Agricultura e Pesca]	Sistemas de Identificação Parcelar/Agriculture Parcels Cultures (Parcels)	2015		*https://publico-isip.ifap.pt/web/Index.aspx*
Copernicus Emergency Management Service (EMS)	Land use maps built under the framework of EMSN018 (EMS)	2015		*https://emergency.copernicus.eu/mapping/list-of-components/EMSN018*
Department of Public Works, Territory and Environment. Autonomous Region of Aosta Valley [Assessorato opere pubbliche, territorio e ambiente. Région Autonome Vallée d'Aoste]	Copertura del Suolo della Valle d'Aosta/Land use VdA (VdA)	2020	CS4	*https://mappe.partout.it/pub/GeoNavSCT/?repertorio=copertura_suolo*
Lesiv, M., Schepaschenko, D., Buchhorn, M. *et al.*	GFMD	2015	All	*https://zenodo.org/record/4541513#.Y6BDCXbMKUm*
OpenStreetMap (OSM)	Solar Plants	Unknown	All	*https://www.openstreetmap.org/*

3.3. Approach and Methods

LULC classification using Sentinel-2 and Landsat-8 imagery is a widely used remote sensing method. Sentinel-2's high spatial resolution enhances differentiation between vegetation, urban areas, and water bodies (Zhang *et al.*, 2022), while Landsat-8's long-term data supports time-series land cover analysis (Huang *et al.*, 2021).

Multi-temporal analysis improves LULC classification accuracy by capturing seasonal vegetation changes. Trimestral Sentinel-2 composites enhance crop and forest classification (García *et al.*, 2023). Additionally, spectral indices like NDVI and NDWI refine classification; NDVI quantifies vegetation health (Jones *et al.*, 2020), while NDWI enhances water detection by suppressing soil and vegetation reflectance (Gao, 1996).

These indices, when integrated into classification models, significantly improve the differentiation between various land cover types. As highlighted by other authors (Liu *et al.*, 2022), "combining NDVI and NDWI with Sentinel-2 and Landsat-8 imagery enhances the accuracy of LULC classifications by reducing spectral confusion among similar classes".

The HR land use maps were produced using a Geographic Object-Based Image Analysis (GEOBIA) approach, which simulates human visual perception by grouping pixels into objects/segments based on context and neighbourhood characteristics. Unlike pixel-based methods, where classification units are uniform pixels, GEOBIA uses image-objects, incorporating statistical, geometrical, and textural data for improved accuracy (Costa *et al.*, 2022). This method is particularly effective for high-resolution image classification and reduces the salt-and-pepper effect, minimizing classification noise. Figure 2 illustrates the workflow applied in the case studies. Figure 2 illustrates the workflow applied in the case studies. Figure 2 shows the workflow applied in the CSs.

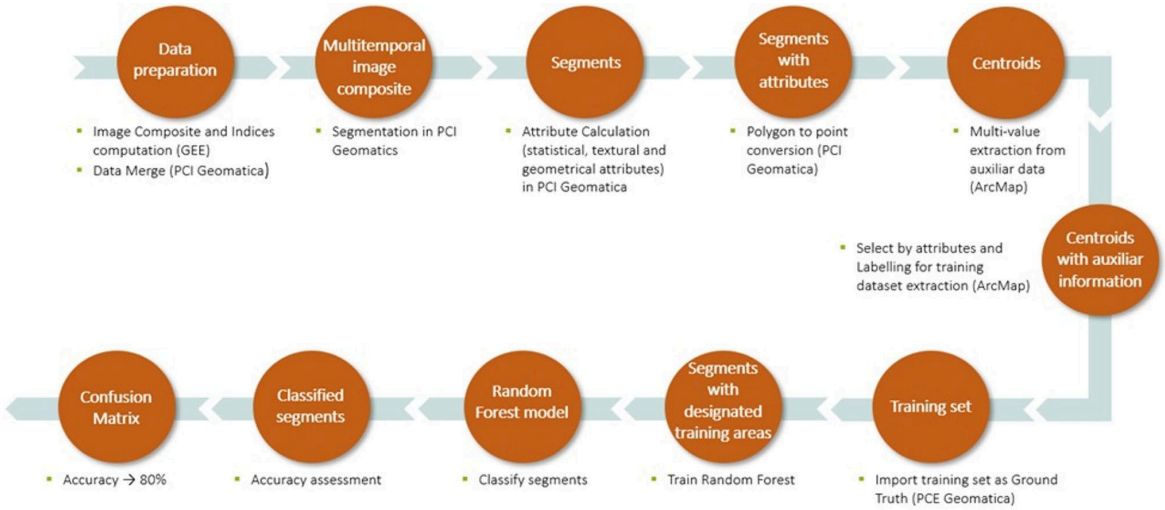

Figure 1. Classification process workflow.

As shown in the figure above, the processes were conducted using Google Earth Engine (GEE), PCI Catalyst Professional (PCI), and ArcMap. GEE was used for satellite imagery compositing (trimestral median values) and indices computation (trimestral maximum values), while PCI handled the GEOBIA process, including data merging, segmentation, attribute calculation, and Random Forest classification. Training sets were extracted and labelled using ArcMap.

Several studies confirm the effectiveness of Sentinel-2 and Landsat-8 for LULC classification. Sentinel-2 excels in urban mapping, while Landsat-8 is better suited for large-scale land cover assessments (Huang *et al.*, 2021). Combining both datasets enhances classification accuracy compared to using either alone (García *et al.*, 2023). The RethinkAction project's methodology, integrating Sentinel-2, Landsat-8, spectral indices, and multi-temporal compositing, aligns with these findings, ensuring high accuracy, particularly for vegetation and water body differentiation, which is essential for suitability mapping in land-based mitigation and adaptation solutions.

3.3.1. Segmentation and Attribute Calculation

The classification process incorporated a 64-layer raster dataset combining auxiliary data and spectral indices to enhance accuracy by capturing spectral, spatial, and temporal characteristics. However, this multi-layered approach introduces redundancy and correlation among variables, potentially causing computational inefficiencies and overfitting (Huang *et al.*, 2021).

To mitigate redundancy, dimensionality reduction techniques like Principal Component Analysis (PCA), Independent Component Analysis (ICA), and Feature Selection Algorithms are commonly used in remote sensing (Duro *et al.*, 2012). While no explicit reduction was applied, these methods were considered in structuring the workflow. Retaining all indices ensures no critical data loss,

though future iterations may explore automated feature selection to enhance efficiency and reduce correlation.

After computing median image composites and indices, they were merged into a 64-channel raster file and used for segmentation. The multiresolution segmentation algorithm in PCI (Ramezan *et al.*, 2021) was applied to generate a vector layer of statistically homogeneous objects, distinguishing them based on spectral and spatial characteristics. The segmentation parameters included:

- Scale: Controls object size; smaller values create more homogeneous, detailed segments, while larger values generate fewer, more heterogeneous objects.
- Shape (0.1–1.0): Adjusts the weight of spectral values, with lower values emphasizing pixel intensity.
- Compactness (0.1–1.0): Defines boundary smoothness, where higher values produce compact objects like crop fields or buildings.

The scale parameter, often the most critical, is typically selected through trial and error (Ramezan *et al.*, 2021). The goal was to create homogeneous segments, minimizing mixed objects to ensure accurate automatic training site extraction based on segment centroids. The chosen parameters were scale: 35, shape: 0.1, and compactness: 0.9.

GEOBIA's advantage over pixel-based classification is its ability to incorporate additional predictors beyond spectral data. PCI computes various spatial and statistical variables, allowing the classification model to determine their relevance. A total of 26 classification features were used:

- Spectral Parameters: Min, max, mean, and standard deviation (STD) were calculated for each band, totaling 256 spectral variables.
- Textural Features: Three co-occurrence-based metrics (mean, entropy, and contrast) were computed using VISIR bands (Red, Green, Blue, Infrared) across all trimesters, resulting in 48 variables. Due to high computational costs, only these key textural features were selected.
- Geometrical Attributes: Nine features (compactness, elongation, circularity, rectangularity, convexity, solidity, form factor, and major/minor axis length) were processed. These are shape-based and require less computational power than spectral or textural measures.
- Vegetation Indices: Ten indices, including NDVI, SAVI, GEMI, and LAI, were computed for the driest trimester, as PCI allowed only one trimester selection.

This approach optimizes classification accuracy while balancing computational efficiency. Overall, a high number of classification features were considered to provide enough information and allow the classification model to decide the relevance of each feature.

3.3.2. Training site extraction

After segmentation, the next step in GEOBIA is training sample collection. Unlike pixel-based approaches, where training areas are polygons delineating individual pixels, object-based image analysis (OBIA) assigns labels to image segments (Khan *et al.*, 2021). This method leverages segment homogeneity, reducing noise and enhancing classification accuracy compared to traditional pixel-based classification (Miranda *et al.*, 2018).

However, the manual extraction of training sites through photointerpretation was deemed unsuitable for this study due to the high number of segments and the large size of the CSs. As highlighted (Hussain *et al.*, 2013), "while manual interpretation remains a valuable tool for high-accuracy training data collection, it is often impractical for large-scale applications due to the high labor and time requirements". Similarly, Blaschke (Blaschke, 2010) emphasized that automated or semi-automated

training sample selection methods are increasingly necessary in large-scale GEOBIA studies to ensure feasibility and consistency in classification.

Given these constraints, alternative automated training site extraction methods have been explored in recent studies, such as machine learning-driven feature selection and rule-based classification strategies, which improve both efficiency and accuracy in LULC classification (Duro *et al.*, 2012).

This is mainly because manual training site extraction is very time consuming and human resource dependent. In addition, there is a lack of local terrain samples and a low spatial resolution of the input data which could not guarantee the quality of the training samples. Therefore, an automatic training site extraction methodology based on previous work of Costa was used (Costa *et al.* 2022).

The computed segments for each CS were converted into centroids and imported into ArcMap. Using the Extract Multi Values to Point tool, these points were assigned attributes from ancillary data for SQL-based labeling. This method requires homogeneous segments to ensure each point represents a single land use class. Labeling was performed through specific queries, e.g., points overlapping CLC Continuous Urban areas, matching local land use maps, and having >80% Imperviousness were classified as Continuous Urban Land. Table 4 illustrates an example of the ArcGIS queries build for the Southern Great Plain CS.

The Solar Land class from OSM was used as an input for training the Solar Land class of the RethinkAction land use maps. The polygons imported from the OSM data were subjected to a visual inspection for refinement before integrating them into the process

Table 4. Queries in ArcGIS applied to the Southern Great Plain CS for point labelling.

Ás que	Nomenclature _Level1	Code_ Level2	Nomenclature_Level 2	Labelling rules
1; 2	Cropland (Rainfed and Irrigated)	1.1; 2.1	Annual	"CLC" in (12) and "OSZ" in(2100,2230) and "IMD" =0 and "WAW"=0 and "TCD" =0 and "GRASS" = 0 or "UAtlas" = 2 and "OSZ" in(2100,2230) and "IMD" =0 and "WAW"=0 and "TCD" =0 and "GRASS" = 0
		1.2; 2.2	Permanent	"CLC" in (15,16) and "OSZ" in (2210,2220) "IMD" =0 and "WAW"=0 and "IBU"=0 and "GRASS"=0 and "WAW"=0 or "UAtlas" = 18 and "OSZ" in (2210,2220) "IMD" =0 and "WAW"=0 and "IBU"=0 and "GRASS"=0 and "WAW"=0
		1.3; 2.3	Pastures	"CLC"=18 and "OSZ" in (3110,3120,3200) and "IBU"=0 and "TCD"=0 and "WAW"=0 and "GRASS"=1 or "UAtlas" =3 and "OSZ" in (3110,3120,3200) and "IBU"=0 and "TCD"=0 and "WAW"=0 and "GRASS"=1
3	Forest	3	Forest	"CLC" in (23,24,25) and "OSZ" in (4301,4302,4303,4304,4305,4306,4307,4308,4309,4401,4402,4403,4403) and "DLT" in (1,2) and "TCD" > 50 and "IMD"=0 and "WAW" = 0 or "UAtlas" =8 and "OSZ" in (4301,4302,4303,4304,4305,4306,4307,4308,4309,4401,4402,4403,4403) and "DLT" in (1,2) and "TCD" > 50 and "IMD"=0 and "WAW" = 0

6	Shrubland	6	Shrubland	"CLC"=29 and "OSZ" in (4502,4600,3500) and "TCD" < 30 and "WAW" =0 and "IMD"=0 or "UAtlas" = 19 and "OSZ" in (4502,4600,3500) and "GRASS"=0 and "TCD"> 30 and "WAW" =0 and "IMD"=0
7	Grassland	7	Grassland	"CLC" = 26 and "OSZ" in (3110,3120,3200,3400,3500) and "GRASS"=1 and "WAW"=0 and "TCD"<15 and "IMD"=0 or "UAtlas"= 19 and "OSZ" in (3110,3120,3200,3400,3500) and "GRASS"=1 and "WAW"=0 and "TCD"<15 and "IMD"=0
8	Wetland	8	Wetlands	"CLC" in (36,35) and "OSZ" in (5110,510,5200) and "WAW" in (3,4) and "IMD"=0 or "UAtlas" =21 and "OSZ" in (5110,510,5200) and "WAW" in (3,4) and "IMD"=0
9	Urban Land	9.1	Continuous	"CLC"=2 and "OSZ" in (1110,1120,1310) and "IMD" > 80 and "IBU"=1 and "TCD"=0 and "GRASS" =0 and "WAW" = 0 or "UAtlas" =1 and "OSZ" in (1110,1120,1310) and "IMD" > 80 and "IBU"=1 and "TCD"=0 and "GRASS" =0 and "WAW" = 0
		9.2	Discontinuous	"CLC"=2 and "OSZ" in (1110,1120,1310) and "IMD" < 80 and "IBU"=1 and "TCD"=0 and "GRASS" =0 and "WAW" = 0 or "UAtlas" in (5,9,11,14) and "OSZ" in (1110,1120,1310) and "IMD" < 80 and "IBU"=1 and "TCD"=0 and "GRASS" =0 and "WAW" = 0
		9.3	Industrial/commercial	"CLC"=3 and "OSZ" in (1110,1120,1310) and "IMD" >60 and "TCD"=0 and "GRASS" =0 and "WAW" = 0 or "UAtlas" = 4 and "OSZ" in (1110,1120,1310) and "IMD" >60 and "TCD"=0 and "GRASS" =0 and "WAW" = 0
		9.4	Mining	"CLC"=7 and "TCD"=0 and "GRASS"=0 and "WAW"=0 or "UAtlas" = 6 and "TCD"=0 and "GRASS"=0 and "WAW"=0
		9.5	Roads/Railways	"OSZ"= 1210 and "IMD">60 and "GRASS"=0 and "TCD" = 0 and "WAW"=0 or "UAtlas" =13 and "IMD">60 and "GRASS"=0 and "TCD" = 0 and "WAW"=0
10	Solar land	10	Solar	Spatial Selection based on OSM data
11	Snow, ice, waterbodies	11	Water	"CLC" in (40,41) and "OSZ" in (6100,6200) and "WAW" in (3,4) and "IMD"=0 and "TCD"=0 and "GRASS"=0 or "UAtlas" = 10 and "OSZ" in (6100,6200) and "WAW" in (3,4) and "IMD"=0 and "TCD"=0 and "GRASS"=0
12	Other land	12	Bare rock/soil/Sparsely vegetated	"CLC" = 32 and "TCD">15 and "GRASS"=1 and "WAW"=0 and "IMD"= 0 or "OSZ" = 4501 and "TCD">15 and "WAW"=0 and "IMD"= 0

The training points are imported as “Ground truth” to PCI. The underlying segments of each labelled point were assigned as training segments and used to train the Random Forest model as explained in the next section.

3.3.3. Random Forest training and Object classification

The Random Forest algorithm is a supervised ensemble machine-learning classifier that constructs multiple decision trees (Breiman, 2001). Each decision tree is generated by randomly selecting a subset of the training data and variables. The effectiveness of the Random Forest approach has been demonstrated in various remote sensing applications, such as land surface temperature downscaling (Tang *et al.*, 2021), highlighting its robustness and supporting its suitability for LULC classification in this study. By introducing randomization into the learning process, the classifier generates multiple models from the same dataset and aggregates their predictions, improving accuracy and reducing overfitting. In other words, after training, each unknown sample is classified based on a majority vote from the ensemble of decision trees, enhancing classification reliability.

Random Forest has gained increasing popularity in remote sensed image classification due to very high accuracies compared to other commonly used classifiers, ease of parametrization, robustness in the presence of noise and its ability to handle high-dimensional datasets (important consideration for multi-spectral object-based analysis) (Costa *et al.*, 2022). The Random Forest classifier was chosen because of two main reasons: the high number of training areas (in theory, the higher the training set, the higher the randomness level, and thus a more efficient learning process is accomplished) and due to the less intensive computation of the classifier compared to other machine-learning classifiers (i.e., Support Vector Machine). Figure 3 shows a simplified schematization of the Random Forest algorithm.

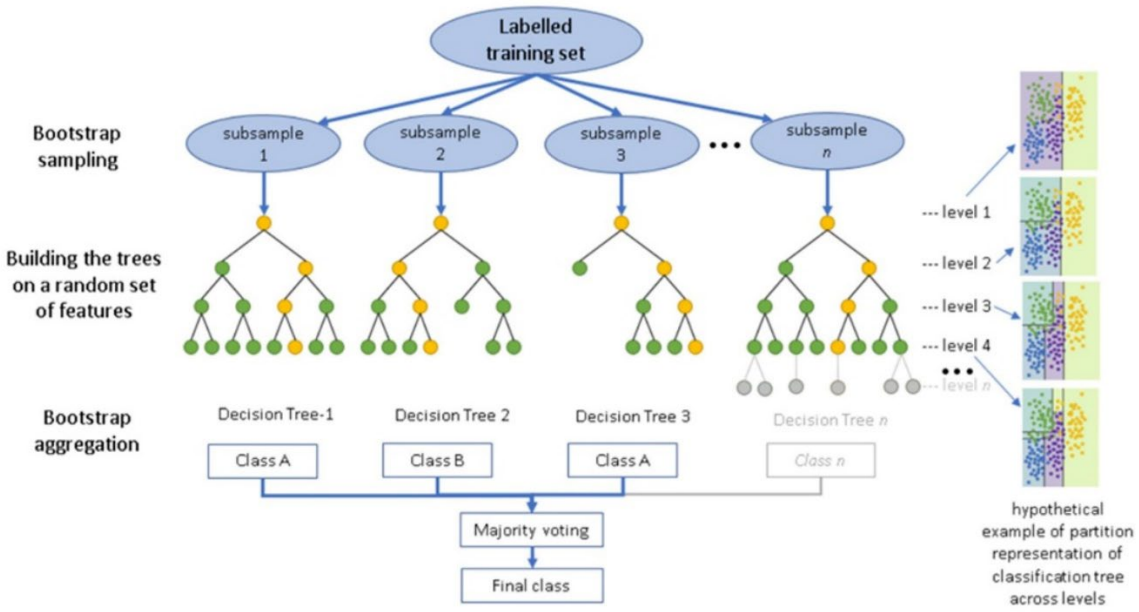

Figure 2: Simplified scheme of the Random Forest algorithm (image extracted from PCI Catalyst Help platform, 2021)

In PCI, the Random Forest classifier uses the OpenCV implementation and uses the following parameters:

- Maximum tree depth: maximum number of levels leaf nodes below the root node.
- Minimum number of samples: minimum number of samples at a leaf node to allow it to be further split into child nodes.
- Active variables: number of randomly selected subset of prediction variables (attributes).

- Tree accuracy (based on the Gini Impurity index): accuracy value used to stop a tree from growing.
- Maximum number of trees: number of trees to generate during the classification process.

The first three parameters determine the split point for a node on each decision tree, while the last two are used as stopping criteria in the Forest growth (both parameters can be used as stopping criteria individually or in a combination of both). The active variable parameter is, by default, set to 0 allowing the classifier to use the square root of the total number of input attributes. The tree accuracy and the maximum number of trees parameters can be used together as stopping criteria (when one is reached the forest stops growing) or can be used individually. Table 5 shows the values for each Random Forest parameter used in the classification of all CSs.

Table 5. Random Forest parameter used in this study.

Random Forest parameter	Parameter value
Max tree depth	20
Min samples count	35
Active variables	0
Max number of trees	500
Trees accuracy	0.05

Max number of trees was set as the stopping criteria and therefore the Trees accuracy was left by default and was not used as a stopping criterion in the Random Forest generation.

3.3.4. Post classification – Forest and Cropland classes

The previous classification method only enables the extraction of the forest class as one single class. Same applicable for cropland class. The lack of ancillary information, the low spatial resolution of the input data and limited resources disable the extraction of sub-classes during the classification process. For the differentiation of the forest area into the three requested forest classes (Forest Managed, Forest Primary, and Forest Plantation) and the cropland classes (Rainfed Cropland and Irrigated Cropland) a post-processing approach was implemented.

For the forest classes, the segments classified as Forest were intersected with the GFMD (see Table 3). In those segments where the auxiliary forest layer (GFMD) did not overlap with the forest mask from the classification, Copernicus Natura 2000 layer (see Table 3) was used to complement the information. Table 6 shows the correspondences between the classes of the global forest management layer, Natura 2000 forest classes and the RethinkAction HR land use classes. Most of the forest mask has been classified using the two referred ancillary datasets, but in some cases small and isolated segments could not be classified. For those segments, a spatial join operation was performed using the closest feature to guide the joining process.

Table 6. Correspondence between ancillary forest layers and RethinkAction HR land use classes.

Global Forest Management Data (GFMD)		
Global Forest Management Code	Global Forest Management classes	RethinkAction HR Land Use classes
11	Naturally, regenerating forest without any signs of human activities, e.g., primary forests	4 - Forest Primary
20	Naturally, regenerating forest with signs of human activities, e.g., logging, clear cuts etc.	3 - Forest Managed

31	Planted forest	3 - Forest Managed
32	Short rotation plantation for timber	5 - Forest Plantation
40	Oil palm plantations	Cropland (not considered)
53	Agroforestry	Cropland (not considered)
Natura 2000 (N2K 2018)		
Natura 2000 Code	Natura 2000 classes	Rethink HR Land Use Classes
4230	Agroforestry	Cropland (not considered)
3110	Natural, semi-natural broadleaved forest	4 - Forest Primary
3120	Highly artificial broadleaved plantations	5 - Forest Plantation
3210	Natural, semi-natural coniferous forest	4 - Forest Primary
3220	Highly artificial Coniferous plantations	5 - Forest Plantation
3310	Natural, semi-natural mixed forest	4 - Forest Primary
3320	Highly artificial mixed plantations	5 - Forest Plantation
3400	Transitional woodland and scrub	4 - Forest Primary
3500	Line of trees and scrub	4 - Forest Primary
3600	Damaged forest	4 - Forest Primary

Regarding cropland classes, the differentiation between rainfed and irrigated croplands was requested for the modelling needs. Several approaches were explored but finally it was decided to use a thresholding of vegetation indices. The selected vegetation indices are: NDVI, NDWI and NDMI. The NDVI is an index that indicates the greenness, density, and health of vegetation in each pixel. Thus, it is suitable for estimating the vegetation vigour throughout the crop cycle. The NDWI reflects moisture in plants and soil and therefore relates strongly with water content, while the NDMI detects moisture levels in vegetation. These indices are commonly used to assess the water stress of vegetation (Haralick, 1979; Wu *et al.*, 2011). The chosen approach is based on thresholding of the vegetation indices during the third trimester of the year as this is a period where the separation between irrigated and rainfed if possible, because of the crop's phenology cycle. Thresholding for rainfed and irrigated cropland differentiation is a well-documented process (Holtgrave *et al.*, 2020). In the Azores archipelago CS, no differentiation was possible due to high values of the indices in analysis and the assumption that no relevant irrigated cropland is present (based on the reference land cover and land use maps as well as the rainfall regime of the region) (You *et al.*, 2013; SNIG, 2018).

Thresholds were defined by trial and error to be adapted to the agroecological conditions of each CS, and the outputs were analysed and validated through visual inspection. Table 7 shows the final thresholds applied on the segments classified as Cropland. Segments with lower values than the indices thresholds shown in Table 7 were classified as rainfed and higher values as irrigated. NDVI was the main driver of the assignation supported by NDWI and NDMI.

Table 7. Thresholds used for Cropland differentiation.

CS	NDVI	NDWI	NDMI
CS1	0.5	0.5	0.3
CS2	0.6	0.55	0.3
CS3	0.45	0.35	0.25
CS4	0.6	0.64	0.2
CS5	0.2	0.25	1.7

3.4. Thematic accuracy assessment

A thematic accuracy assessment of all HR land use maps was conducted using a stratified random sampling approach to ensure an unbiased and representative validation process. The methodology followed these key steps:

- Stratified random sampling was applied to ensure that the sample was randomly distributed, reducing human bias.
- The sample was stratified per class to guarantee that all land use categories had a nonzero probability of inclusion.
- Validation points were generated randomly without classification information and labeled through visual photointerpretation by independent experts following a "four-eyes" review process.
- One hundred validation points per class were initially used, with a minimum of 20 points for smaller land cover classes to ensure statistical significance.
- Sample stratification was based on class area, meaning larger land cover types were assigned proportionally more validation points.
- Due to limited validation data, the three forest classes (Forest Managed, Forest Primary, and Forest Plantation) were validated as a single forest class to improve classification reliability.

3.4.1. Accuracy Metrics and Confusion Matrix Analysis

The classification accuracy was assessed by comparing the mapped features against a reference database (ground truth), obtained through visual interpretation of satellite imagery. A confusion matrix was produced to calculate:

- Overall Accuracy (OA) – The proportion of correctly classified points across all land use classes.
- Producer Accuracy (PA) – The likelihood that a reference land cover type is correctly classified in the final map (indicating omission errors).
- User Accuracy (UA) – The probability that a classified land cover type matches the real-world category (indicating commission errors).

Table 8 presents the OA, PA, and UA values extracted from the confusion matrices for each CS at both classification levels L1 and L2.

Table 8. OA, PA, UA confusion matrices summary table.

Case Study (CS)	L1 OA (%)	L2 OA (%)	L1 PA Range (%)	L1 UA Range (%)	L2 PA Range (%)	L2 UA Range (%)
CS1	**85**	**83**	67 - 95	72 - 98	65 - 93	70 - 96
CS2	**86**	**86**	23 - 97	57 - 100	20 - 95	55 - 98
CS3	**94**	**91**	71 - 99	74 - 99	68 - 97	72 - 98
CS4	**95**	**90**	69 - 100	60 - 100	65 - 98	58 - 99
CS5	**84**	**82**	59 - 96	60 - 100	55 - 95	57 - 98
CS6	**93**	**91**	70 - 98	73 - 99	68 - 96	70 - 98

The accuracy results demonstrate strong classification performance, with Overall Accuracy (OA) ranging from 82% to 95% across different CSs.

- The highest accuracy was observed in CS4 at L1 (95%) and CS3 at L2 (91%), reflecting well-differentiated land cover types in these regions.
- Producer Accuracy (PA) indicates that certain land cover classes had higher omission errors, particularly in CS2 where PA values ranged from 23% to 97%.
- User Accuracy (UA) remained consistently high, with values exceeding 99% in some categories, particularly in CS6 and CS3, indicating strong classification reliability.

4. Results and discussion

The created HR land use maps are in line with the requirements defined by the project in terms of spatial resolution, land use classes, spatial coverage and overall accuracy. The input data are as recent as possible to provide a full temporal and spatial coverage of the Areas of Interest (AOIs) dealing with unavailability of free cloud composites in part of the areas.

Figure 4 to 15 present the High Resolution (HR) land use maps for levels L1 and L2 across the six RethinkAction case studies (CS1–CS6). These case studies span diverse biogeographical regions in Europe and represent a wide range of land use dynamics and environmental conditions. The maps provide a detailed baseline for spatial analysis and scenario modelling.

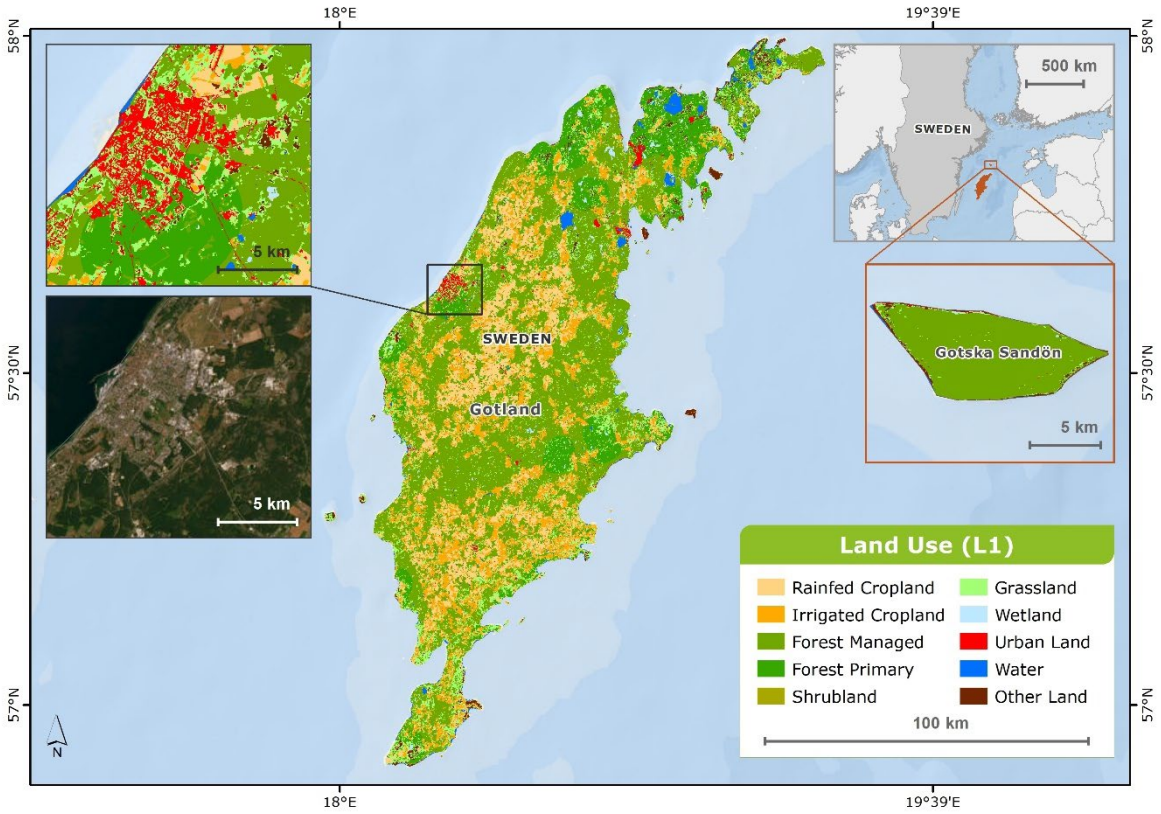

Figure 4: L1 HR land use map of CS1–Gotland Region.

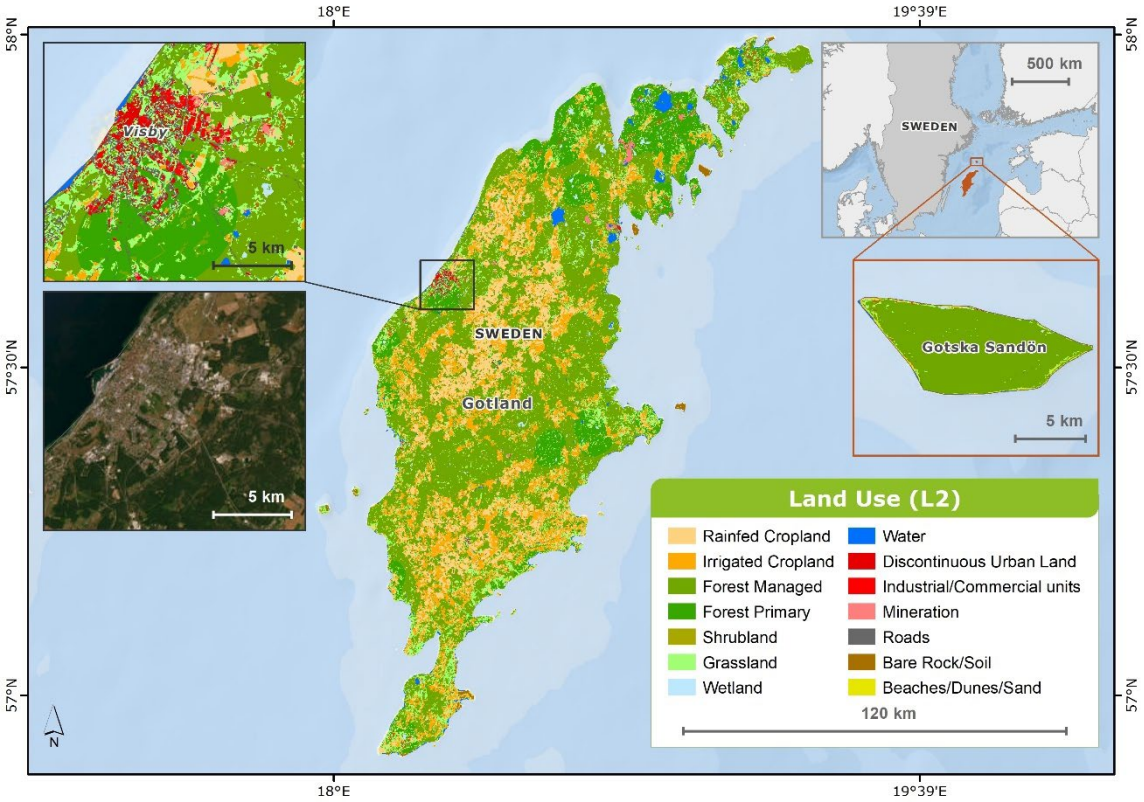

Figure 5: L2 HR land use map of CS1–Gotland Region.

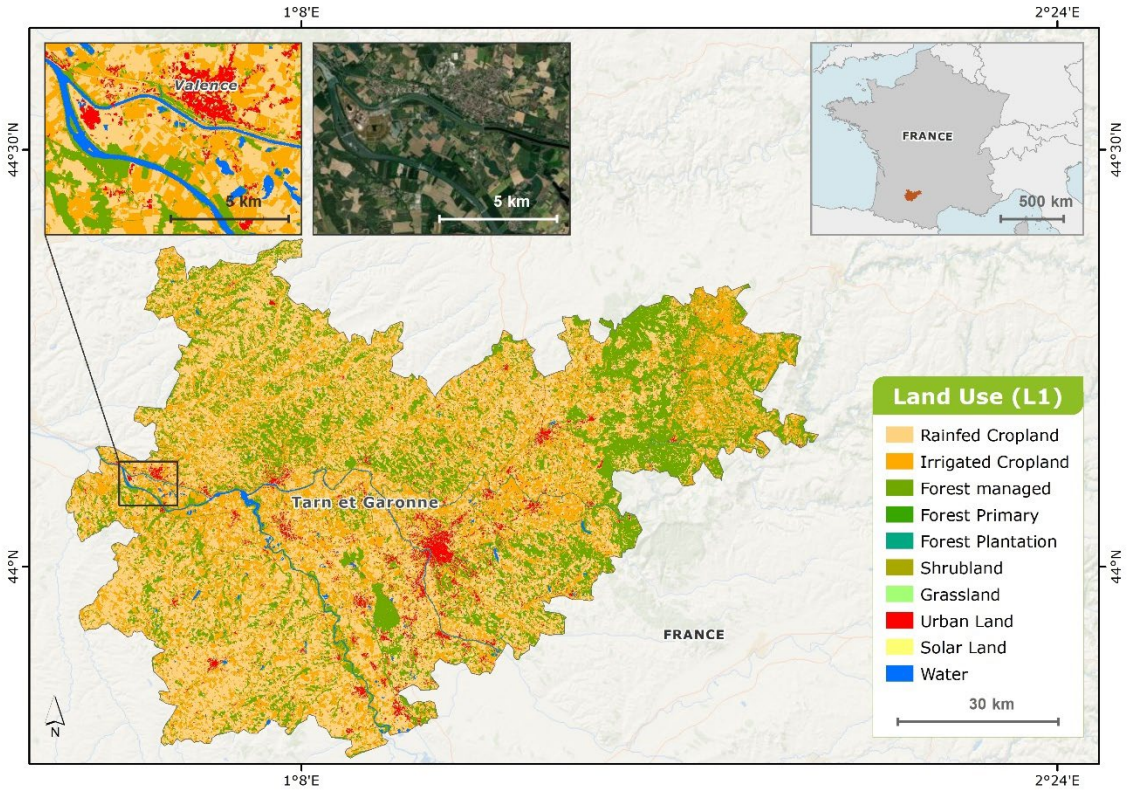

Figure 6: L1 HR land use map of CS2–Tarn-et-Garonne.

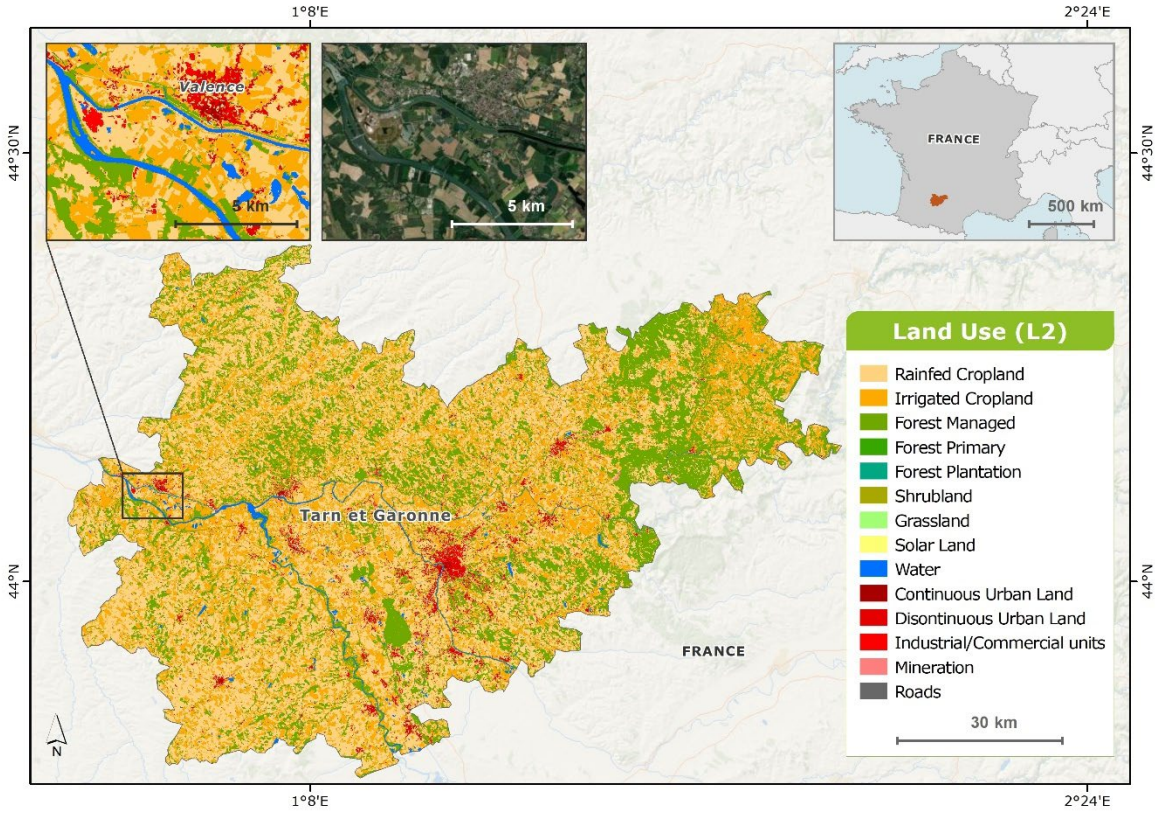

Figure 7: L2 HR land use map of CS2–Tarn-et-Garonne.

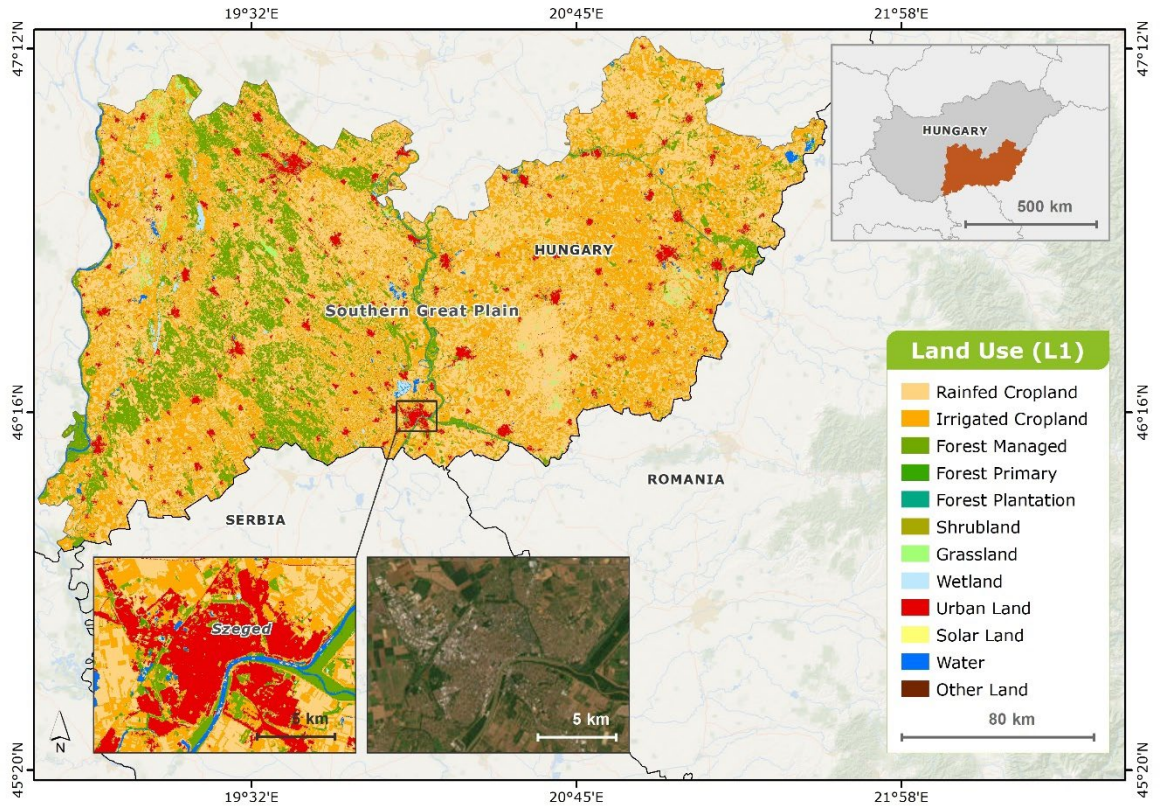

Figure 8: L1 HR land use map of CS3–Southern Great Plain.

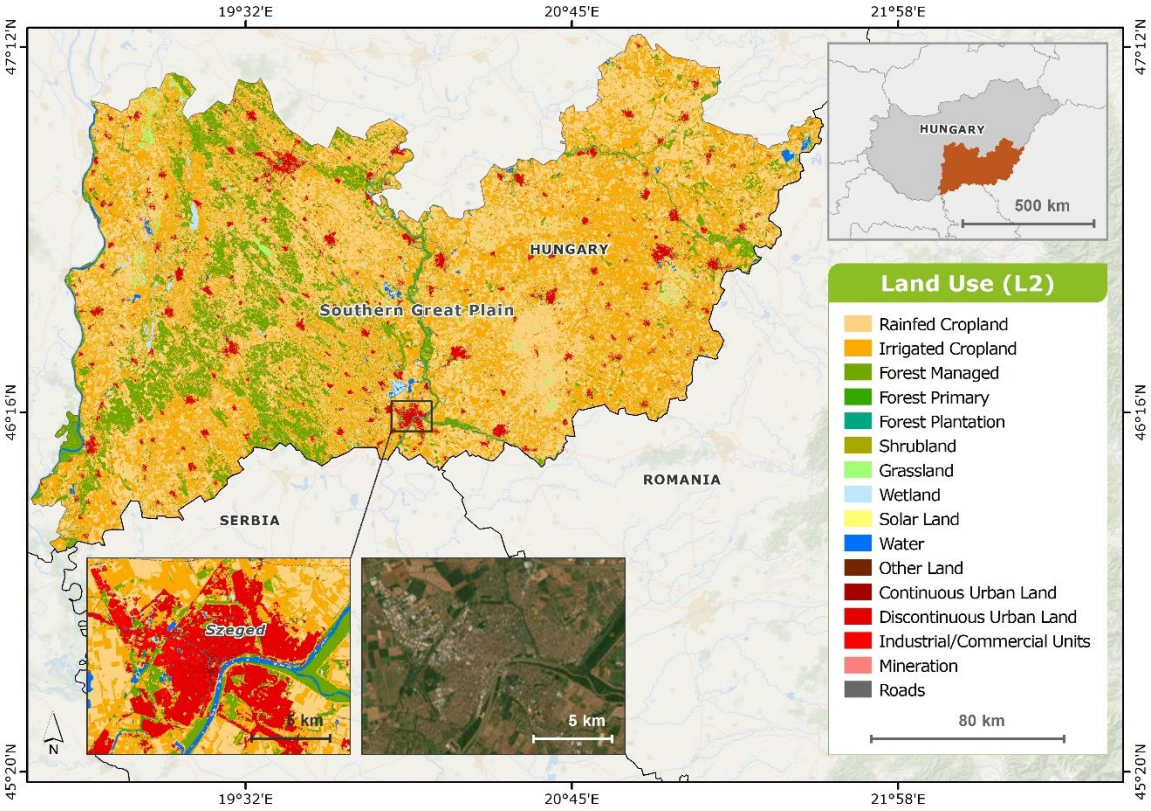

Figure 9: L2 HR land use map of CS3–Southern Great Plain.

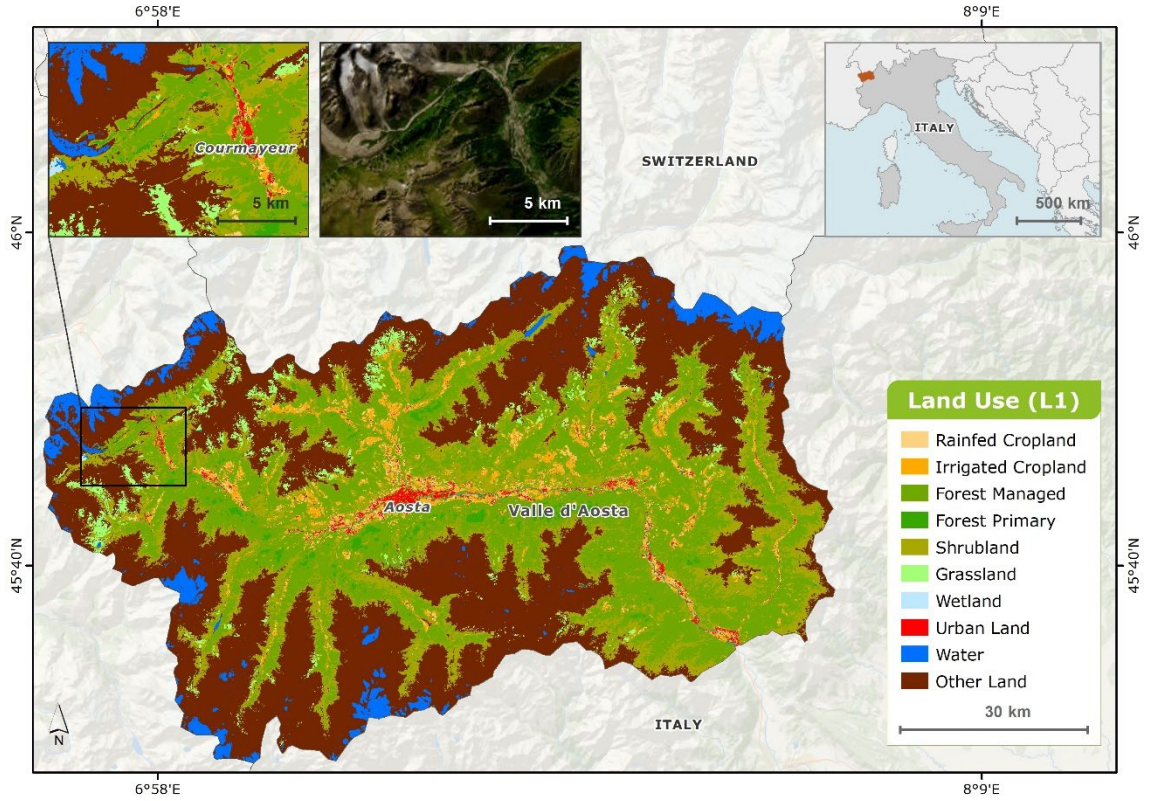

Figure 10: L1 HR land use map of CS4–Valle d'Aosta Region.

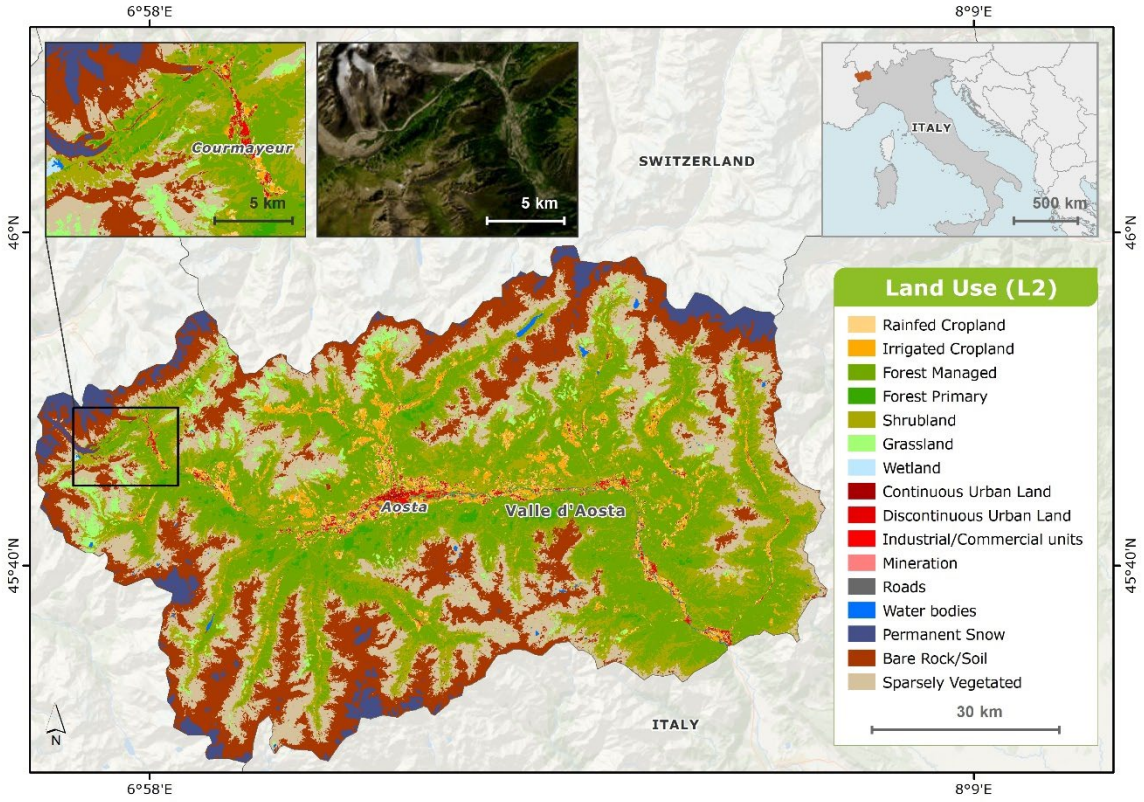

Figure 11: L2 HR land use map of CS4–Valle d'Aosta Region.

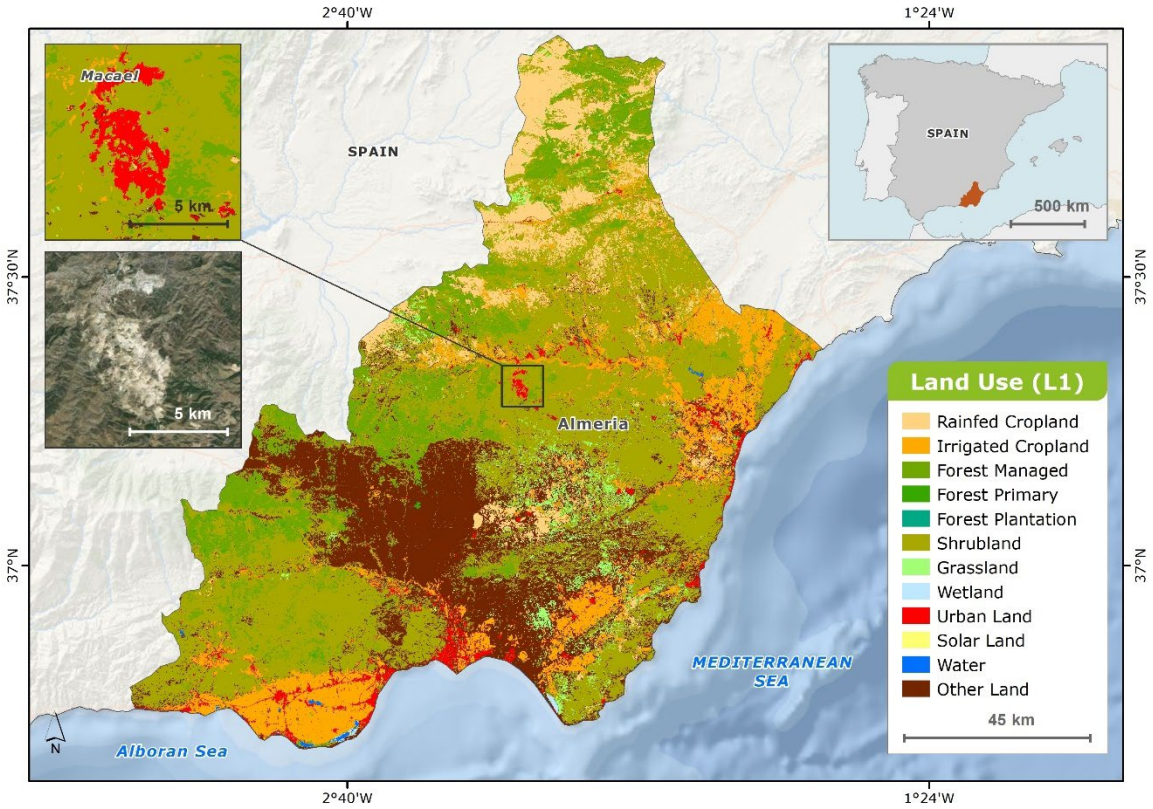

Figure 12: L1 HR land use map of CS5–Almería Province.

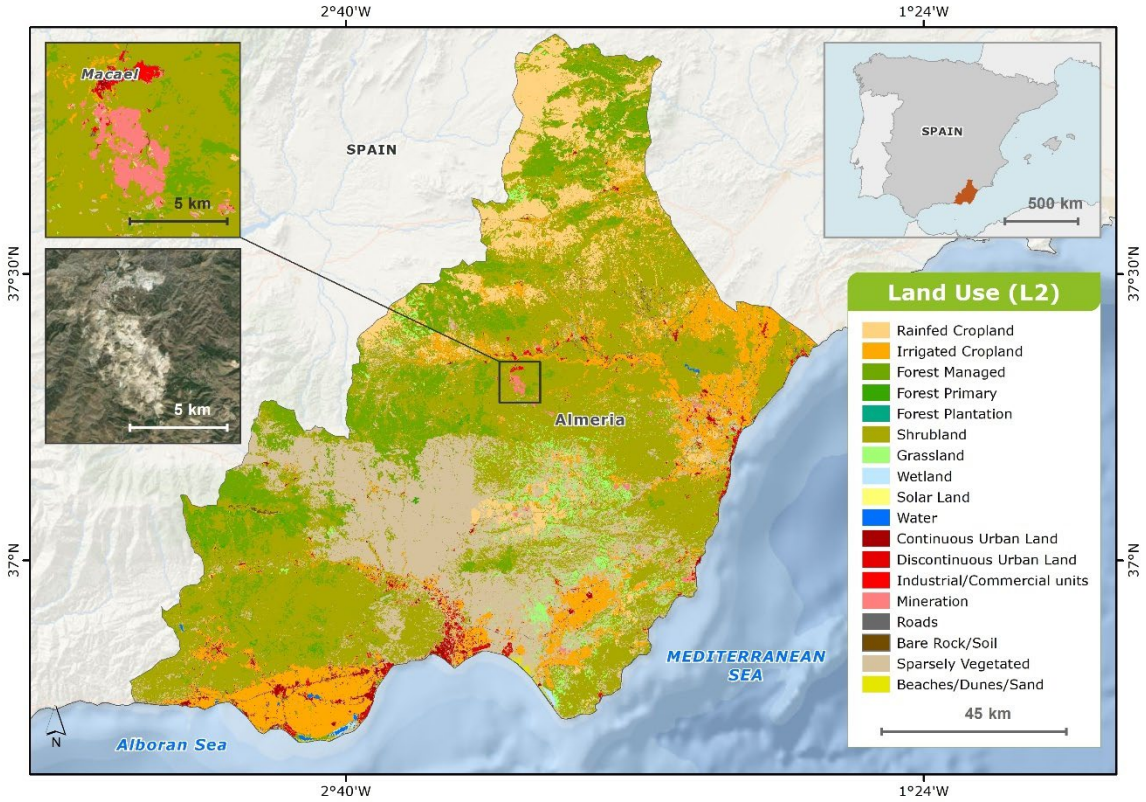

Figure 13: L2 HR land use map of CS5–Almería Province.

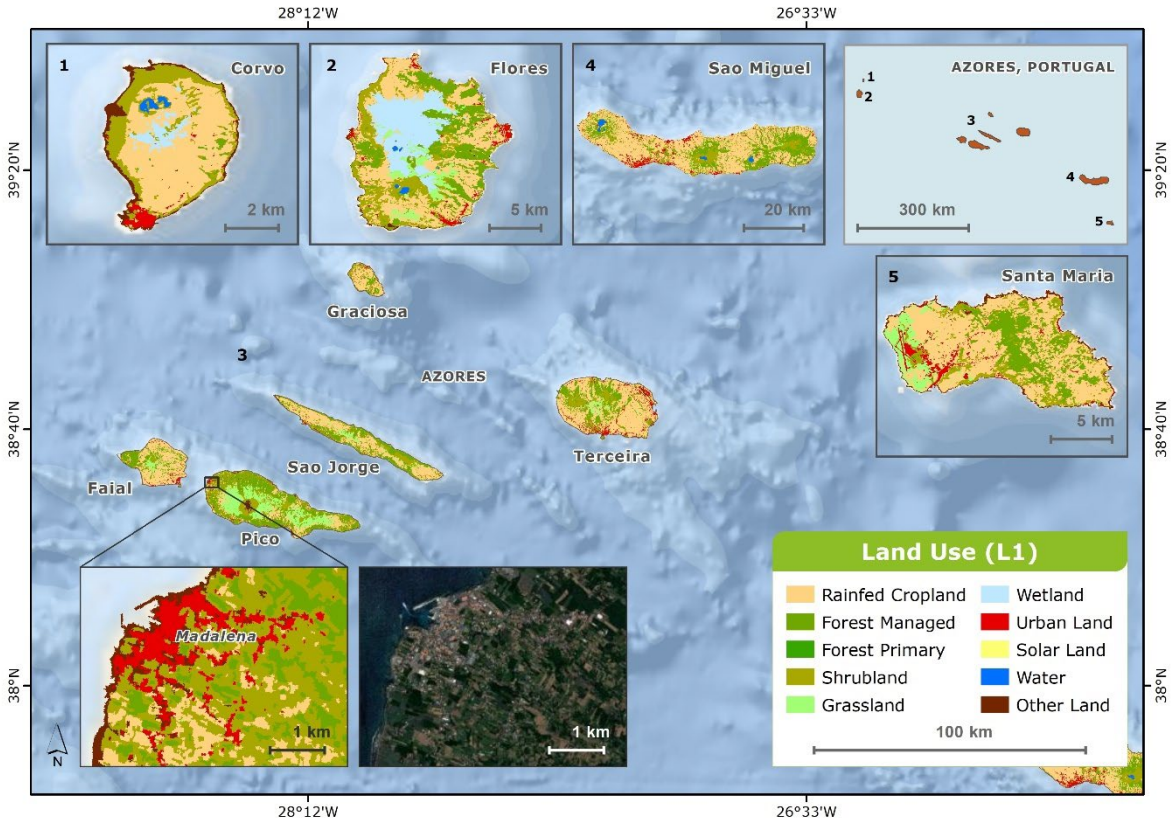

Figure 14: L1 HR land use map of CS6–Azores Archipelago.

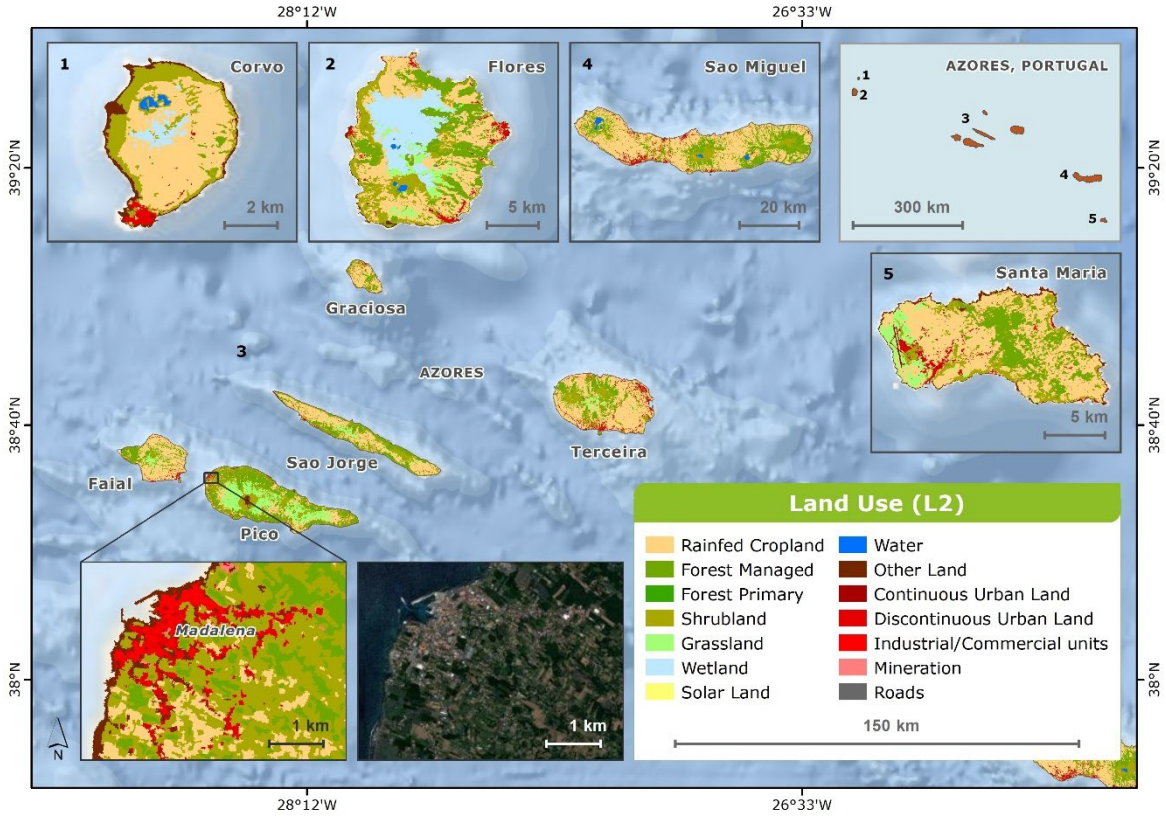

Figure 15: L2 HR land use map of CS6–Azores Archipelago.

All high-resolution land use maps are available in geospatial format for download from the project's Zenodo repository (RethinkAction Project, 2024)

Although relatively simple, the methodology seems robust and scientifically solid. However, the following improvements can be considered:

- Data used, especially in multitemporal approaches, are usually very large. A potential reduction of the number of bands could be explored to lighten the data size, making the process more efficient and avoiding data redundancy.
- For enhance computing and modelling efficiency, dimensionality reduction/classification feature selection techniques could be applied to feed the Random Forest model (a step that could be explored is exploratory data analysis (EDA) and Feature Engineering).
- An alternative classification based in a hierarchical logic could be considered to improve the results. Binary masks can be generated starting from water and non-water, then from non-water to extract vegetation and non-vegetation areas and so on.
- Training criteria could be reviewed and consequently refined as needed. To guarantee the quality of the training data, a random selection (10%) could be chosen and visually inspected.
- The possibility to distinguish additional classes such as pastures could be considered for future work if needed.

5. Conclusions

This study has detailed the creation and application of HR land use maps developed within the RethinkAction H2020 project. These maps serve as a fundamental baseline for analyzing land-based

adaptation and mitigation capacities, providing essential inputs for the project's scenario modeling and spatial assessments.

A key advancement in this study is the use of the RF machine-learning classifier, which has demonstrated its robustness, reliability, and superior accuracy in remote sensing applications (Breiman, 2001; Liu *et al.*, 2022). The ensemble learning nature of RF ensures better handling of high-dimensional datasets, a critical factor in object-based classification (Duro *et al.*, 2012). As highlighted by Costa *et al.* (2022), the integration of Random Forest with GEOBIA significantly reduces classification errors and salt-and-pepper noise, enhancing thematic accuracy and replicability of land use classifications.

The replicability of the proposed methodology is a notable outcome, as it allows for adaptation to different geographical areas with minimal modifications. The study demonstrates that the use of auxiliary data covering all or most CSs facilitates scalability and broader applicability. However, as identified in previous studies, local datasets with higher spatial resolution may be required in specific contexts to refine classification results (Duro *et al.*, 2012). Future applications of this methodology will need to identify and incorporate region-specific datasets to further enhance classification accuracy.

The RethinkAction HR land use maps provide a valuable resource for multiple applications. Beyond their immediate use in the project's scenario modeling, these maps are the cornerstone for the generation of suitability maps, which guide decision-making in land-based climate change adaptation and mitigation strategies. These suitability maps will enable stakeholders to assess which regions are most suitable for specific land use transitions, ensuring efficient resource allocation and sustainable development (ESA, 2024). Additional future analyses should focus on further refining the suitability mapping process by integrating multi-criteria decision analysis (MCDA) and machine learning-based spatial modeling approaches.

Further research should explore the integration of dimensionality reduction techniques, such as Principal Component Analysis (PCA) or Feature Selection Algorithms, to optimize the classification workflow and reduce redundancy in multi-layered datasets (Huang *et al.*, 2021). Additionally, future studies could investigate hierarchical classification approaches and alternative machine-learning models to further refine classification accuracy and processing efficiency.

In conclusion, the study provides the required HR land use maps, supporting the production of suitability maps and ensuring that the RethinkAction decision-making platform can provide data-driven insights for sustainable land management and climate adaptation. The established method provides a robust and replicable land use classification approach that can be implemented for further work. These findings contribute to the broader goal of sustainable land use planning and provide actionable insights for policymakers, researchers, and practitioners in the field of climate change mitigation and adaptation.

Acknowledgements

This work was carried out within the framework of the project "RethinkAction", that received funding from the European Union's Horizon 2020 research and innovation programme under Grant Agreement No. 101037104.

References

Azores: National Geographic Information System (SNIG). Regional Secretariat for the Environment and Climate Change/Government of the Azores. 2018. *Carta de Ocupação do Solo de 2018 - Região Autónoma dos Açores (RAA)* [Cartography]. 1:25:000.

Beshir, S., Moges, A., Donato, M. 2023. Trend analysis, past dynamics and future prediction of land use and land cover change in upper Wabe-Shebele river basin. *Heliyon, 9*. https://doi.org/10.1016/j.heliyon.2023.e19128

Blaschke, T. 2010. Object based image analysis for remote sensing. *ISPRS Journal of Photogrammetry and Remote Sensing, 65*(1), 2-16. https://doi.org/10.1016/j.isprsjprs.2009.06.004

Breiman, L. 2001. Random forests. *Machine Learning, 45*(1), 5–32. https://doi.org/10.1023/A:1010933404324

Costa, H., Benevides, P., Moreira, F.D., Moraes, D., Caetano, M. 2022. Spatially stratified and multi-stage approach for national land cover mapping based on Sentinel-2 data and expert knowledge. *Remote Sensing, 14*, 1865. https://doi.org/10.3390/rs14081865

Duro, D.C., Franklin, S.E., Dube, M.G. 2012. A comparison of pixel-based and object-based image analysis with selected machine learning algorithms for the classification of agricultural landscapes using SPOT-5 HRG imagery. *Remote Sensing of Environment, 118*, 259-272. https://doi.org/10.1016/j.rse.2011.11.020

European Space Agency (ESA). 2024. Land use mapping is an invaluable tool in the realm of climate change mitigation, serving as a foundational element for greenhouse gas inventories. Retrieved from https://climate.esa.int/de/neuigkeiten-und-veranstaltungen/high-resolution-maps-reveal-real-world-land-use-change/

Gao, B.C. 1996. NDWI—A normalized difference water index for remote sensing of vegetation liquid water from space. *Remote Sensing of Environment, 58*(3), 257-266. https://doi.org/10.1016/S0034-4257(96)00067-3

García, M.L., Torres, R.J., Silva, D.P. 2023. Evaluating Sentinel-2 and Landsat-8 imagery for land cover classification in heterogeneous landscapes. *Remote Sensing Applications: Society and Environment, 27*, 100375. https://doi.org/10.1016/j.rsase.2023.100375

Gong, P., Wang, J., Yu, L., Zhao, Y., Zhao, Y., Liang, L., ..., Chen, J. 2020. Finer resolution observation and monitoring of global land cover: First mapping results with Landsat TM and ETM+ data. *International Journal of Remote Sensin*g, 41(6), 2000–2022. https://doi.org/10.1080/01431161.2020.1724202

Hansen, M.C., Potapov, P.V., Moore, R., Hancher, M., Turubanova, S.A., Tyukavina, A., ..., Townshend, J.R. G. 2013. High-resolution global maps of 21st-century forest cover change. *Science*, 342(6160), 850–853. https://doi.org/10.1126/science.1244693

Haralick, R.M. 1979. Statistical and structural approaches to texture. *Proceedings of the IEEE, 67*(5), 786-804.

Holtgrave, A.K., Röder, N., Ackermann, A., Erasmi, S., Kleinschmit, B. 2020. Comparing Sentinel-1 and -2 data and indices for agricultural land use monitoring. *Remote Sensing, 12*(18), 2919. https://doi.org/10.3390/rs12182919

Huang, X., Li, J., Zhang, J. 2021. A comparative assessment of Landsat-8 and Sentinel-2 for land cover classification in urban environments. *International Journal of Remote Sensing, 42*(18), 3576-3592. https://doi.org/10.1080/01431161.2021.1911432

Hussain, M., Chen, D., Cheng, A., Wei, H., Stanley, D. 2013. Change detection from remotely sensed images: From pixel-based to object-based approaches. *ISPRS Journal of Photogrammetry and Remote Sensing, 80*, 91-106. https://doi.org/10.1016/j.isprsjprs.2013.03.006

Jones, B., Kumar, S. 2020. The use of NDVI in land cover classification: A review of applications and challenges. *Journal of Remote Sensing & GIS, 9*(2), 29-41. https://doi.org/10.1080/01431161.2020.1850203

Khan, H., Ali, I. 2021. Geographic Object-Based Image Analysis for Small Farmlands Using Sentinel-2 Imagery. *Pakistan Journal of Science, 72*(1), 1-10. https://doi.org/10.53560/PPASA(60-1)795

Liu, H., Wang, Z., Chen, Y. 2022. Integrating spectral indices and machine learning for accurate land cover classification: A case study using Sentinel-2 and Landsat-8. *ISPRS Journal of Photogrammetry and Remote Sensing, 189*, 12-28. https://doi.org/10.1016/j.isprsjprs.2022.02.006

Miranda, H.D., Mutiara, A.B. 2018. Classification of land cover from Sentinel-2 imagery using supervised classification technique: Preliminary study. *Proceedings of the 2018 International Conference on Applied Engineering (ICAE)*, 1-5. https://doi.org/10.1109/INCAE.2018.8579398

Patankar, N., Sarkela-Basset, X., Schivley, G., Leslie, E., Jenkins, J. 2022. *Land use trade-offs in decarbonization of electricity generation in the American West*. arXiv preprint.

PCI Catalyst Help platform. 2021. Retrieved from https://catalyst.earth/catalyst-system-files/help/

PCI Geomatics Enterprises, Inc. 2022. Retrieved from https://catalyst.earth/catalyst-system-files/help/

Ramezan, C.A., Warner, T.A., Maxwell, A. E., Price, B.S. 2021. Effects of training set size on supervised machine learning land-cover classification of large-area high-resolution remotely sensed data. *Remote Sensing, 13*, 368. https://doi.org/10.3390/rs13030368

RethinkAction Project (2024). RethinkAction project. CRoss-sEcToral planning decisIoN-maKing platform to foster climate Action. Retrieved from https://zenodo.org/communities/rethinkaction/

Tang, K., Zhu, H., Ni, P. 2021. Spatial downscaling of land surface temperature over heterogeneous regions using random forest regression considering spatial features. *Remote Sensing, 13*, 3645. https://doi.org/10.3390/rs13183645

Wu, W., De Pauw, E. 2011. A simple algorithm to identify irrigated croplands by remote sensing. *Proceedings of the 34th International Symposium on Remote Sensing of Environment (ISRSE)*, Sydney, Australia (pp. 10-15). Arinex.

You, X., Meng, J., Zhang, M., Dong, T. 2013. Remote sensing-based detection of crop phenology for agricultural zones in China using a new threshold method. *Remote Sensing, 5*(7), 3190-3211. https://doi.org/10.3390/rs5073190

Zhang, Q., Yu, X., Tang, W. 2022. Advances in remote sensing-based land cover classification: A review of Sentinel-2 and Landsat-8 applications. *Environmental Monitoring and Assessment, 194*, 123. https://doi.org/10.1007/s10661-022-09879-7

Zhao, X., Tan, W., Guo, H., Wang, L., Wu, X. 2022. Urban expansion monitoring using Sentinel-2 imagery and deep learning methods. *Remote Sensing*, 14(2), 398. https://doi.org/10.3390/rs14020398